

Fig. S1: Combination and number of significant PCs for the different precipitation regions for the 95<sup>th</sup> quantile in autumn (A), winter (B) and spring (C).

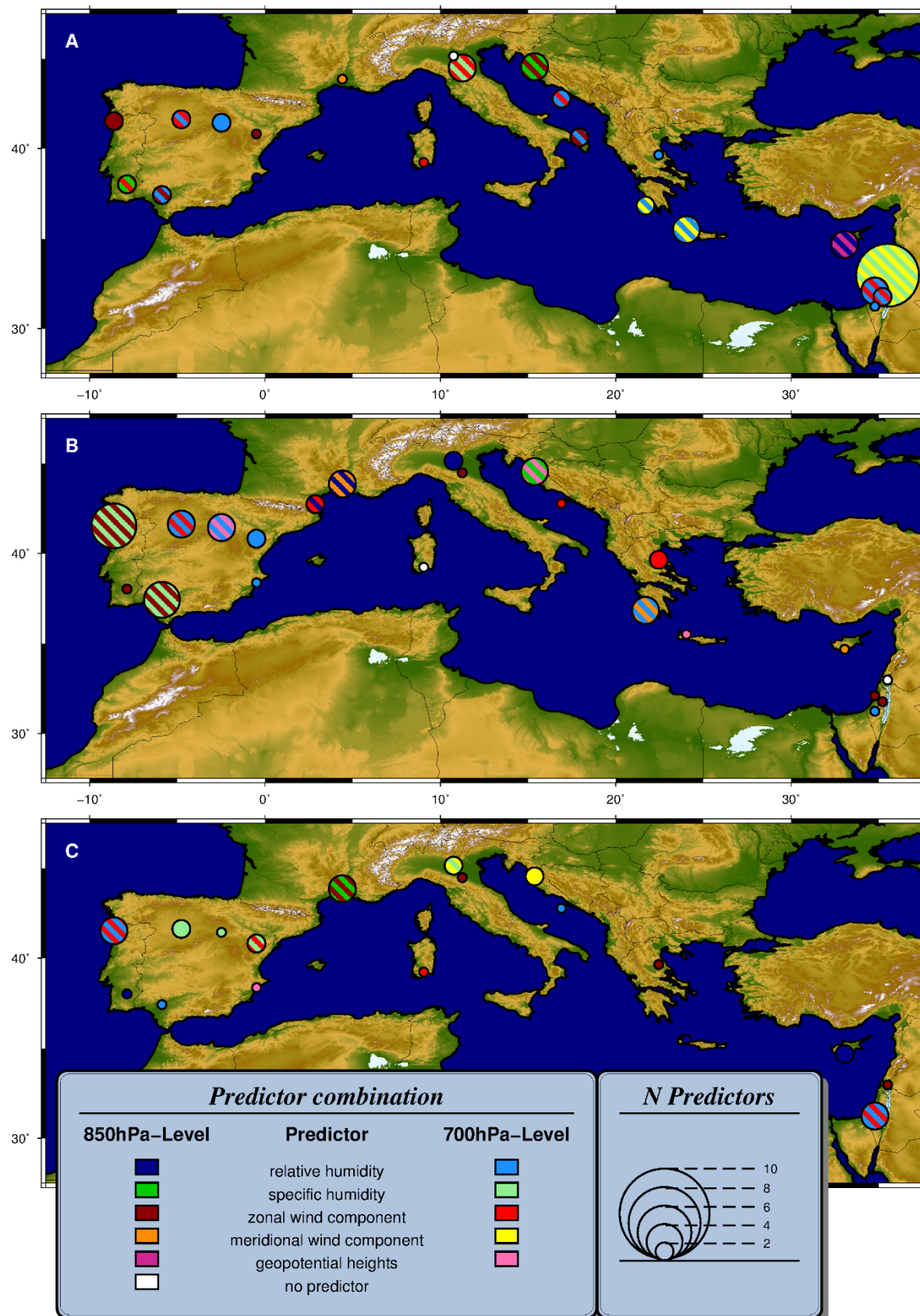


Fig. S2: Combination and number of significant PCs for the different precipitation regions for the 99<sup>th</sup> quantile in autumn (A), winter (B) and spring (C).

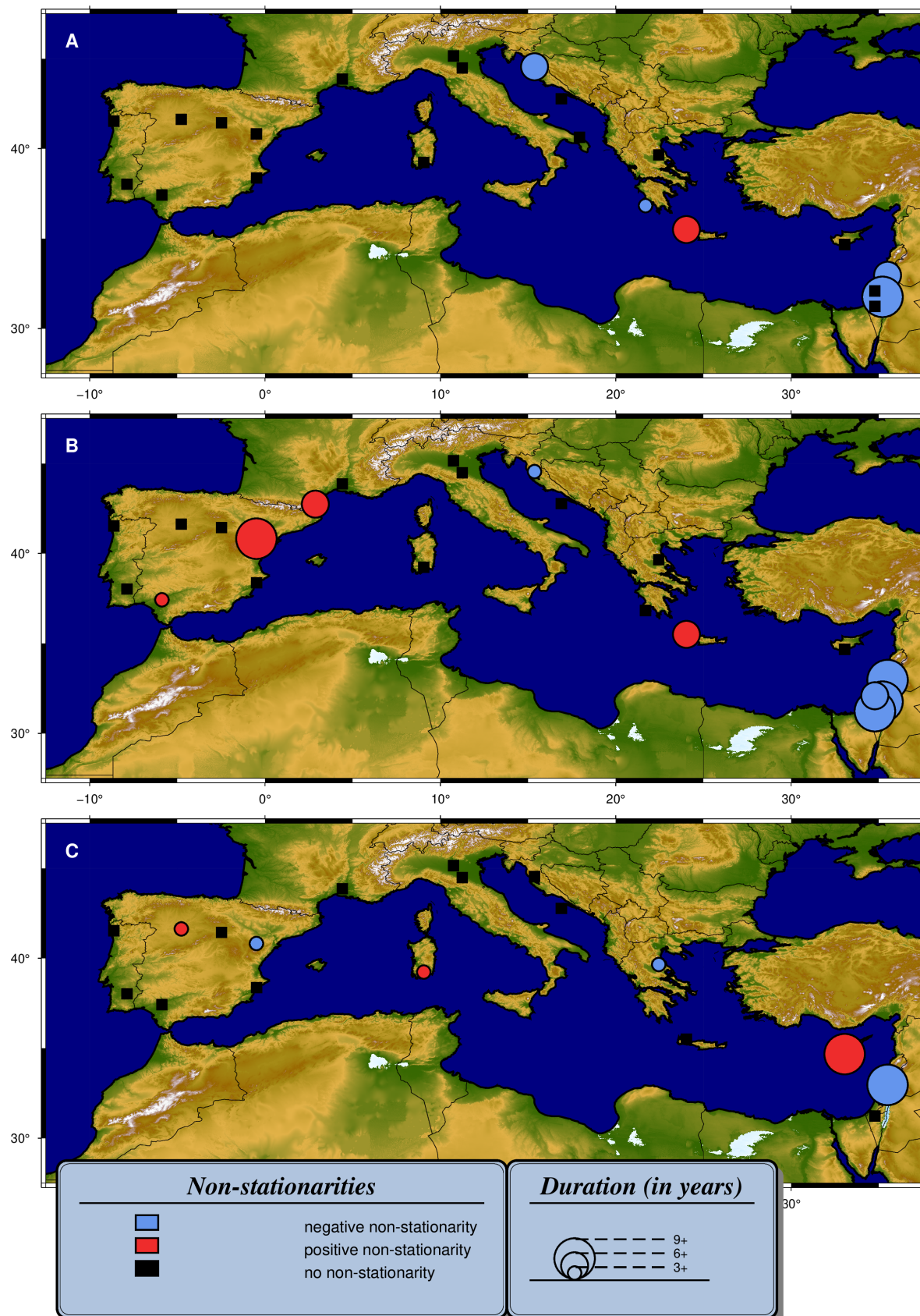


Fig. S3: Overview of non-stationary predictor-predictand-relationships in the Mediterranean area for the 95<sup>th</sup> quantile in autumn (A), winter (B) and spring (C).

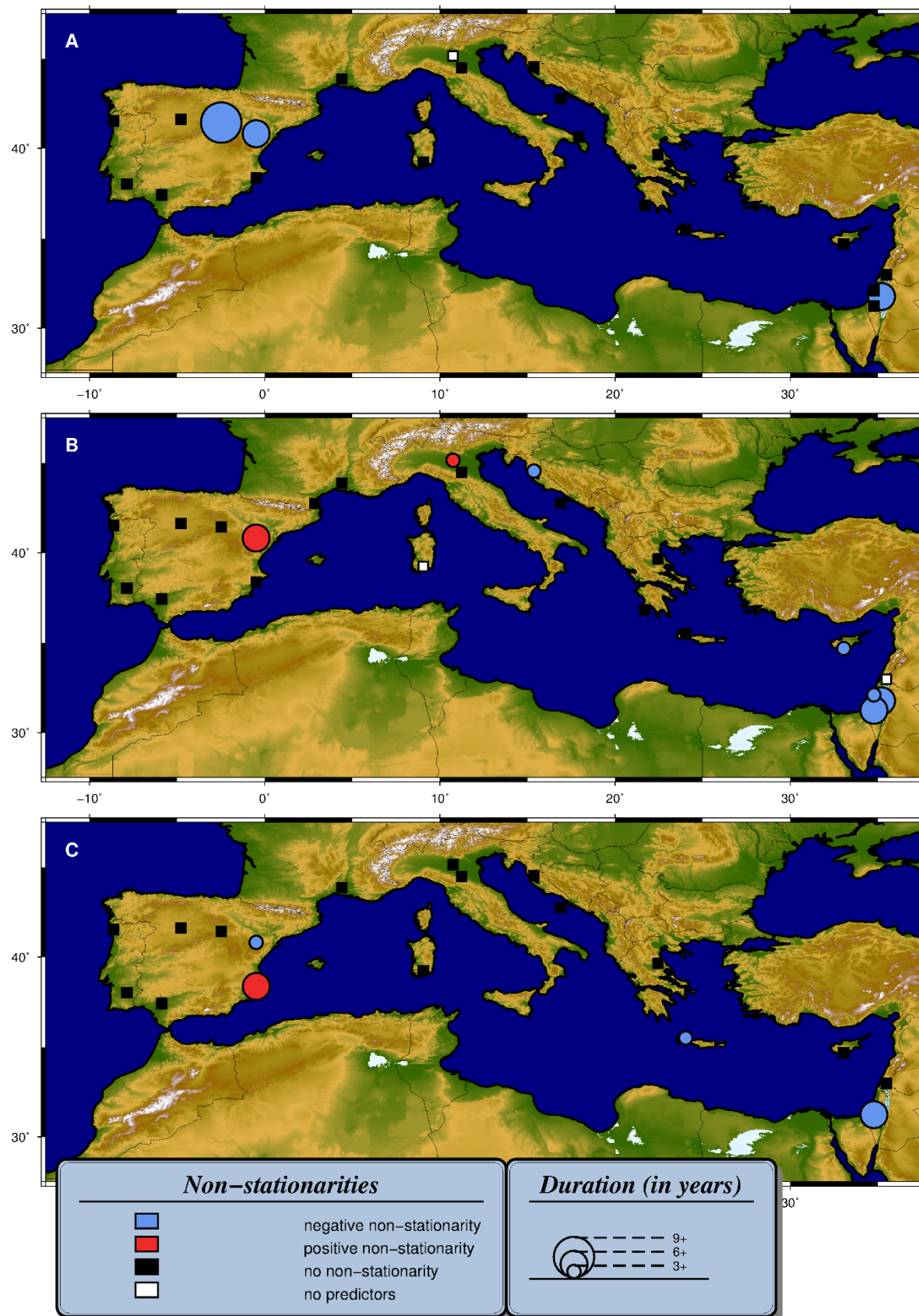


Fig. S4: Overview of non-stationary predictor-predictand-relationships in the Mediterranean area for the 99<sup>th</sup> quantile in autumn (A), winter (B) and spring (C).

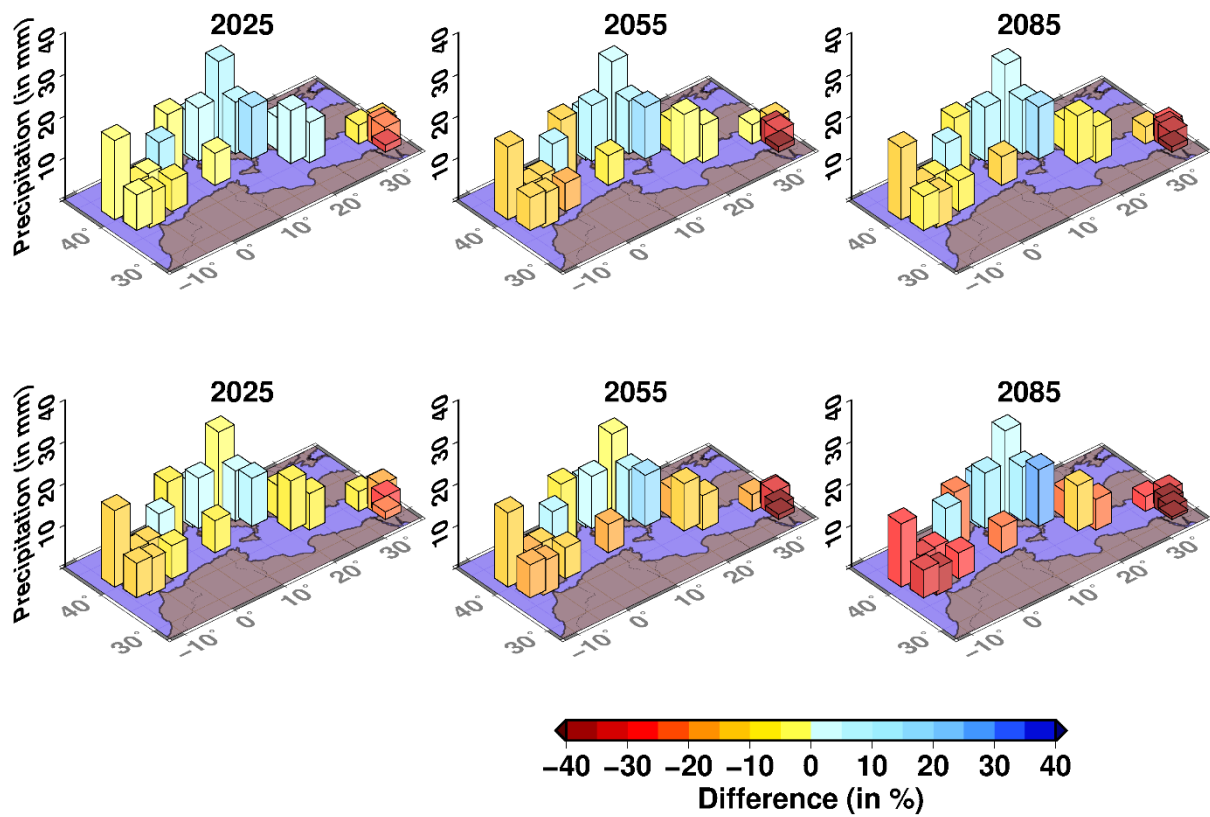


Fig. S5: Assessments of Q95 for all reference stations of the Mediterranean area in autumn under RCP4.5 (top) and RCP8.5 (bottom) of MPI-ESM-LR for the early (period 2025: 2010-2040), mid (period 2055: 2040-2070) and late (period 2085: 2070-2100) 21<sup>st</sup> century. Absolute quantile values are displayed with bars, relative changes in comparison with the mean of the historical runs are displayed in colors.

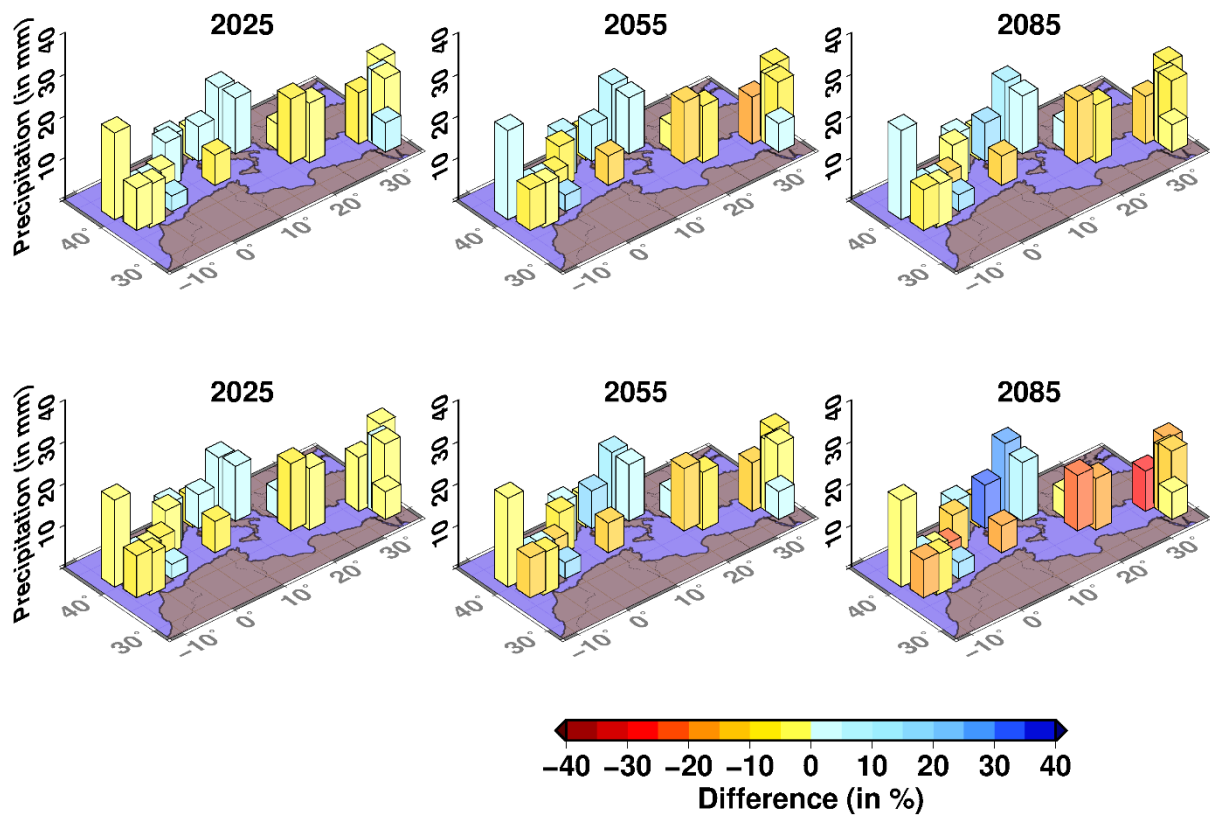


Fig. S6: Same as Fig. S5, but for winter.

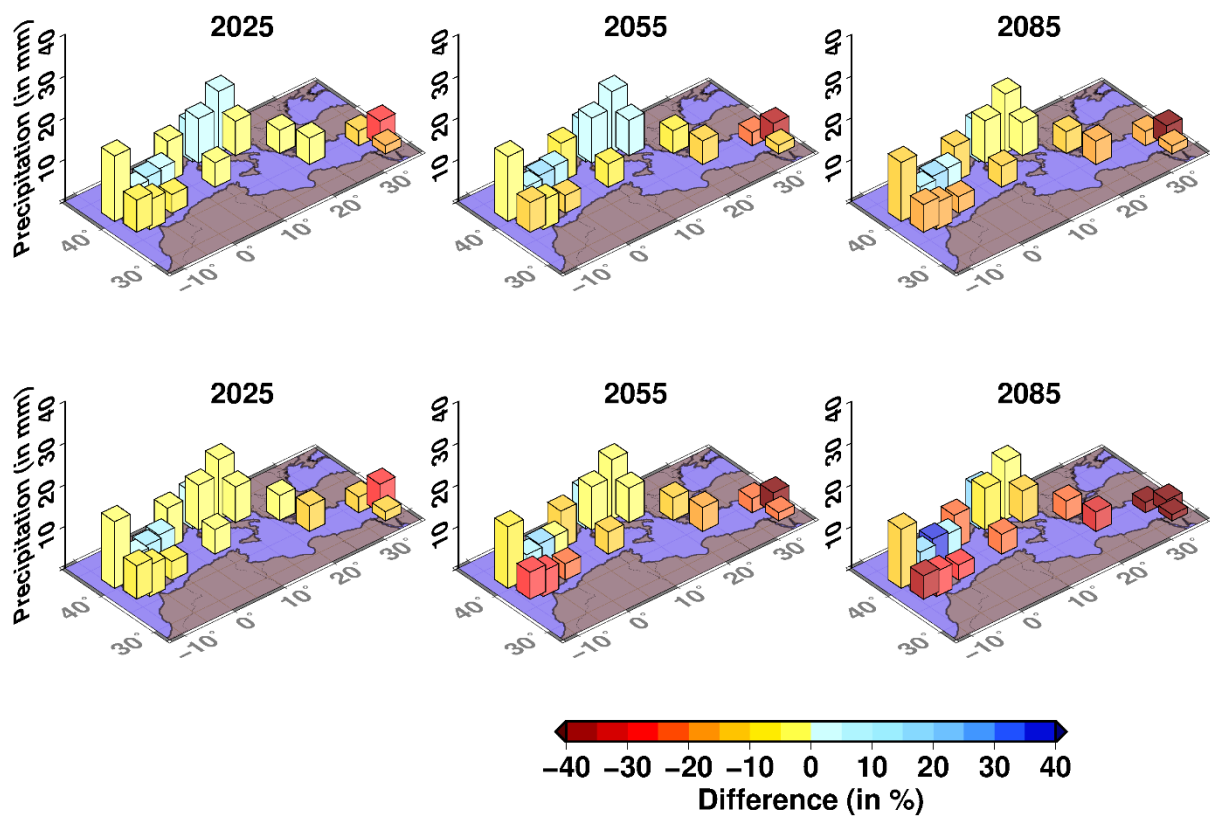


Fig. S7: Same as Fig. S5, but for spring.

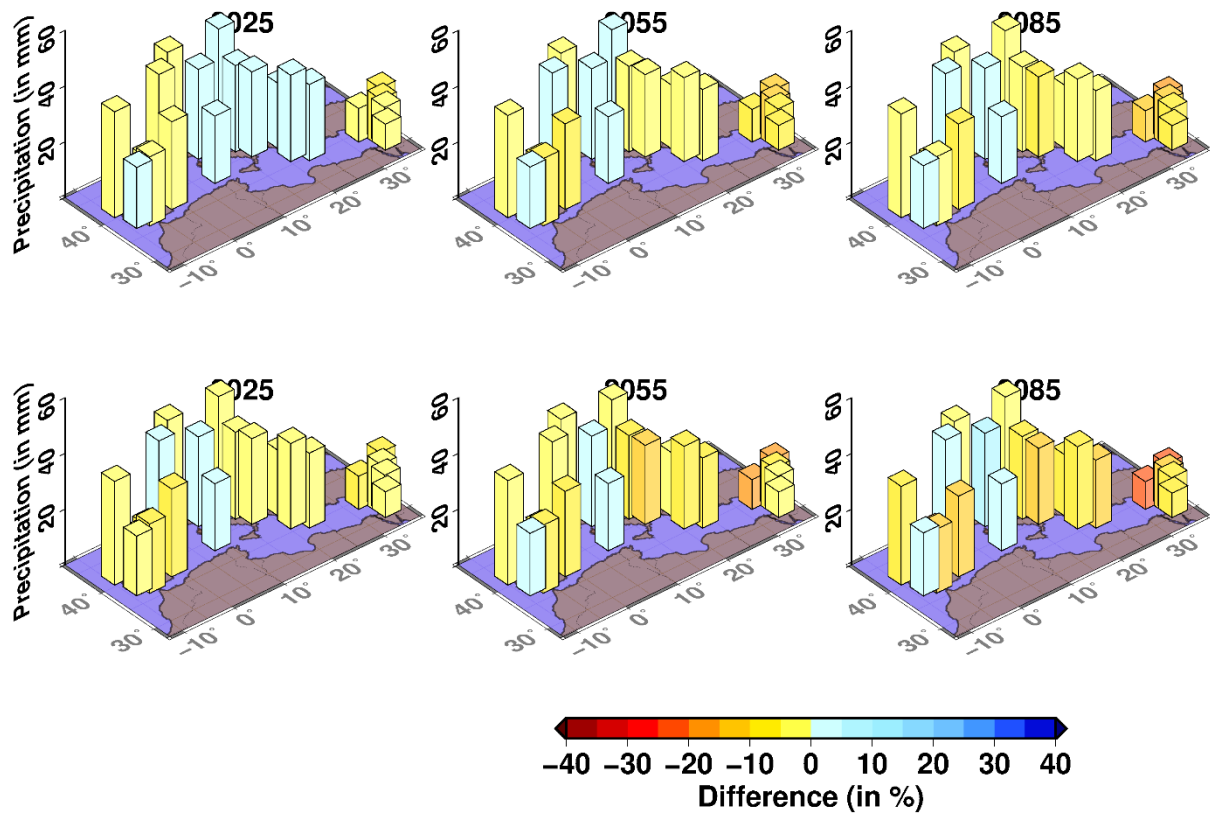


Fig. S8: Assessments of Q99 for all reference stations of the Mediterranean area in autumn under RCP4.5 (top) and RCP8.5 (bottom) of MPI-ESM-LR for the early (period 2025: 2010-2040), mid (period 2055: 2040-2070) and late (period 2085: 2070-2100) 21<sup>st</sup> century. Absolute quantile values are displayed with bars, relative changes in comparison with the mean of the historical runs are displayed in colors.

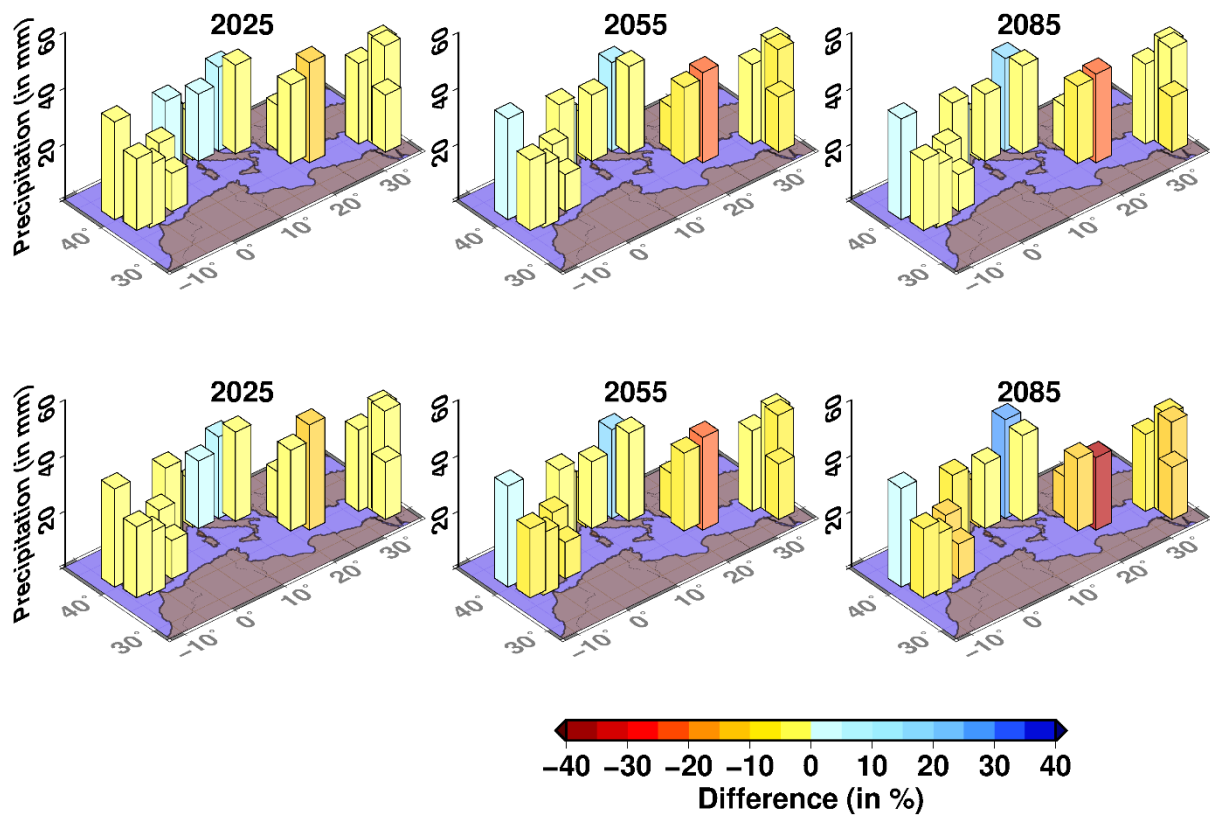


Fig. S9: Same as Fig. S8, but for winter.

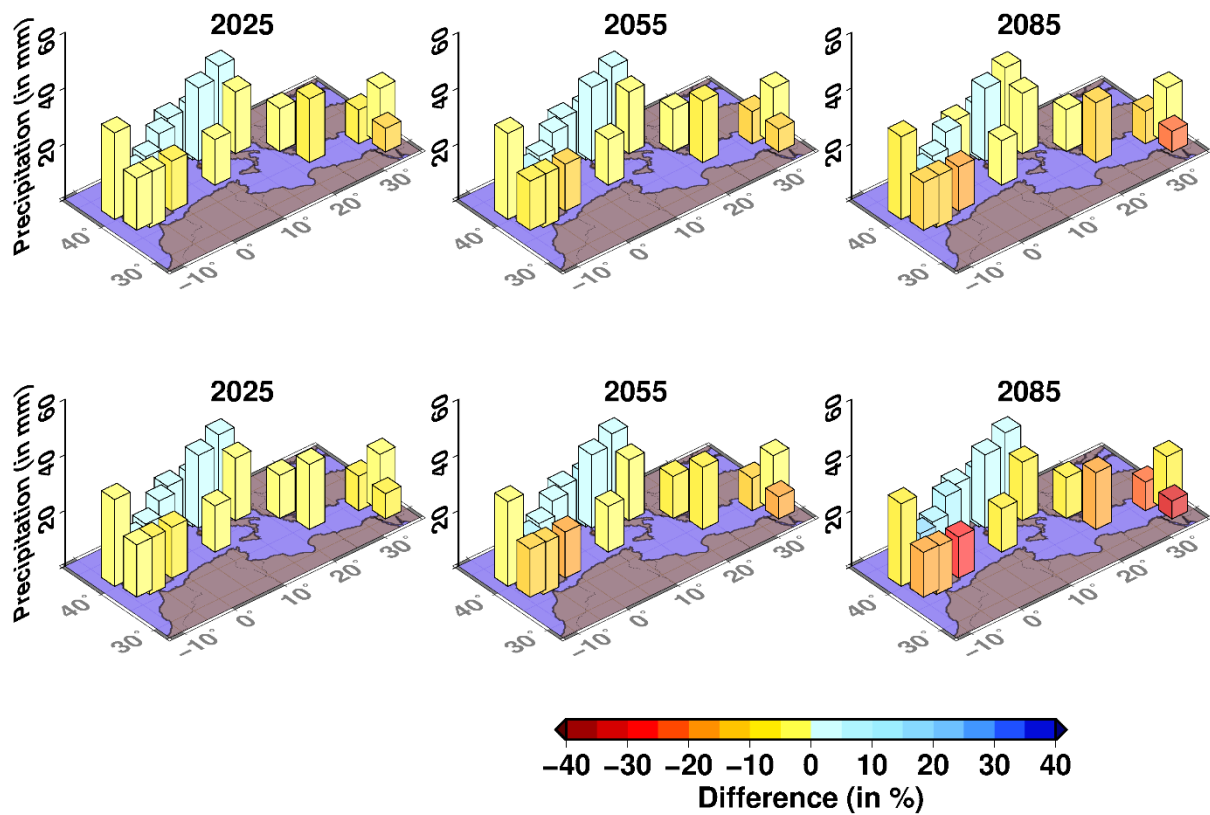


Fig. S10: Same as Fig. S8, but for spring.